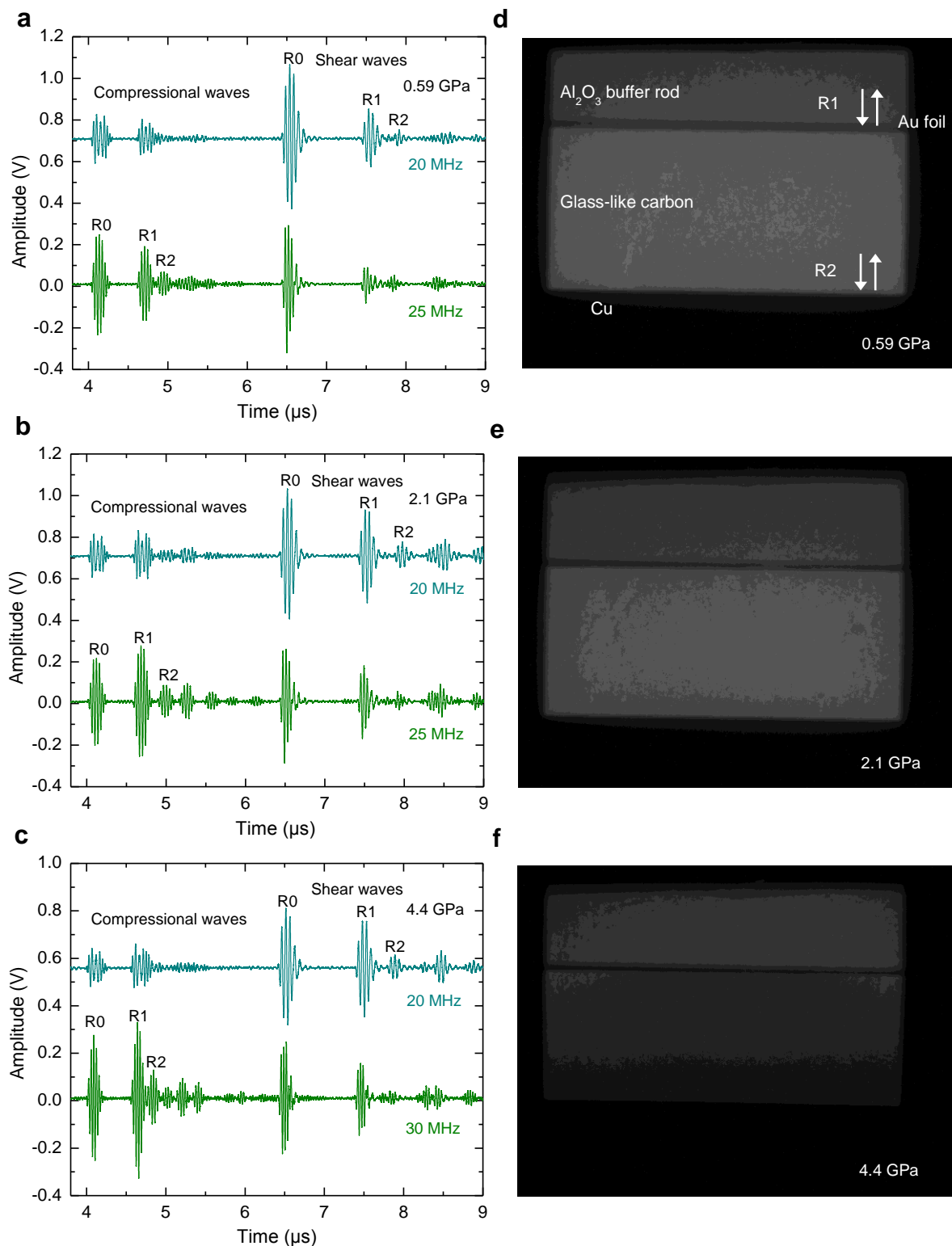
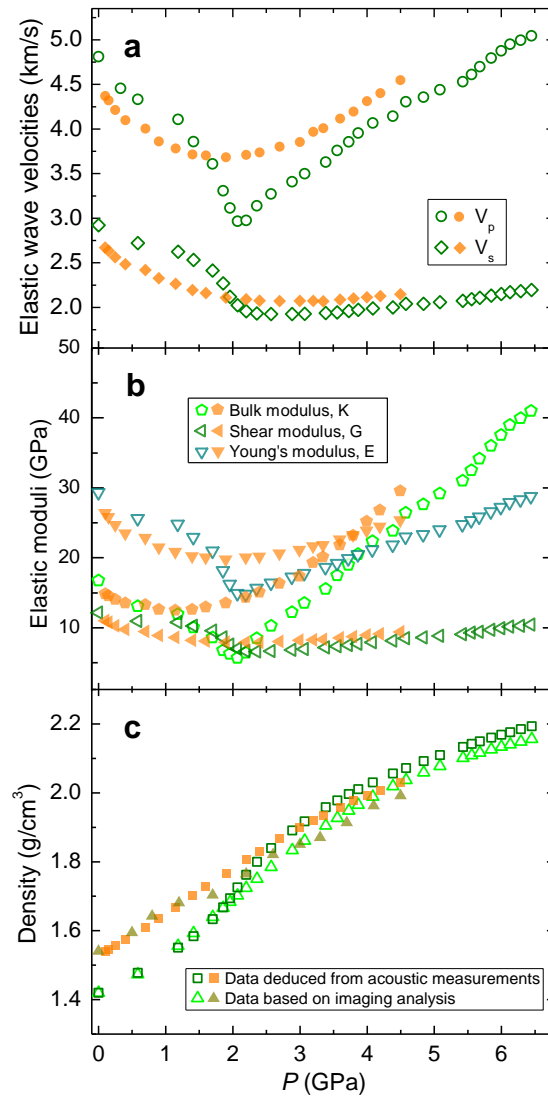


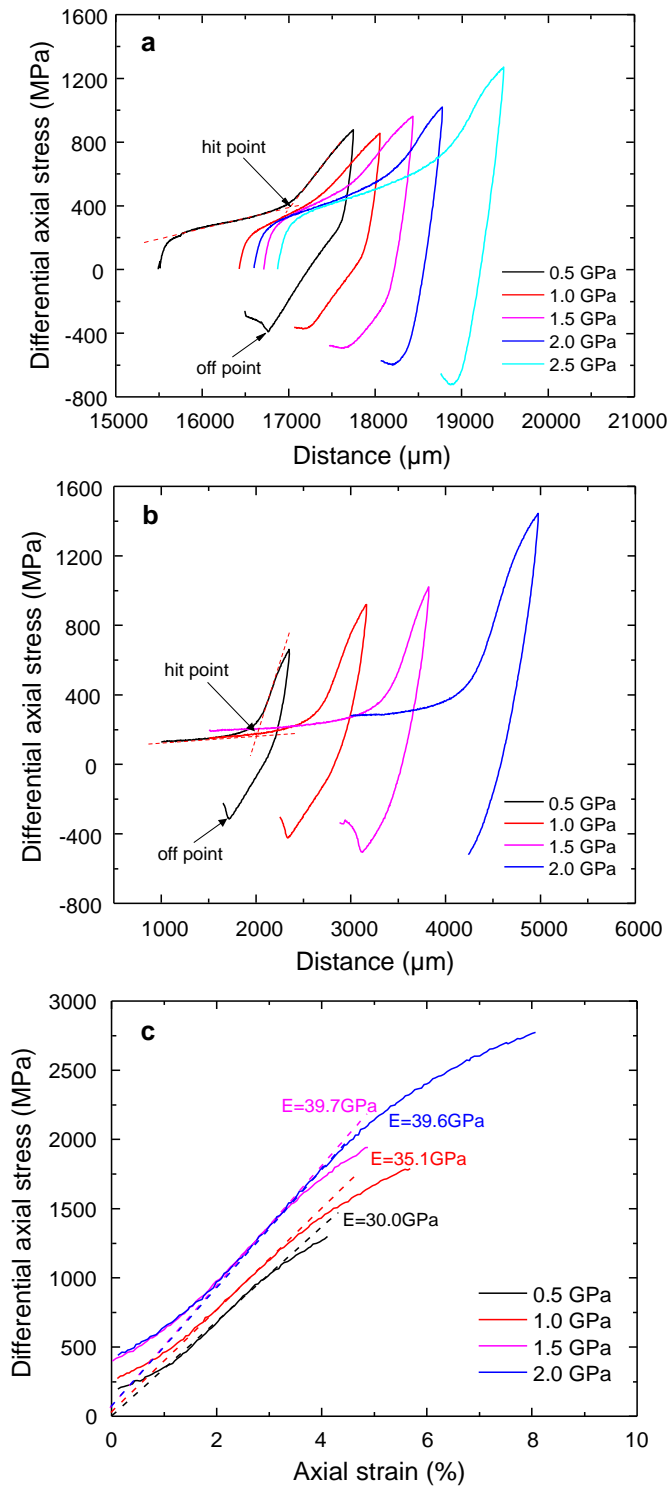
Supplementary Figure 1 | Compression behavior of type-II glass-like carbon (GC) under hydrostatic pressure. (a) An example of recorded sample images in a diamond anvil cell during compression and decompression. Arrows indicate directions of pressure change. (b) Pressure (P) - volume (V) relations upon compression to 35.5 GPa and decompression using helium as pressure medium.



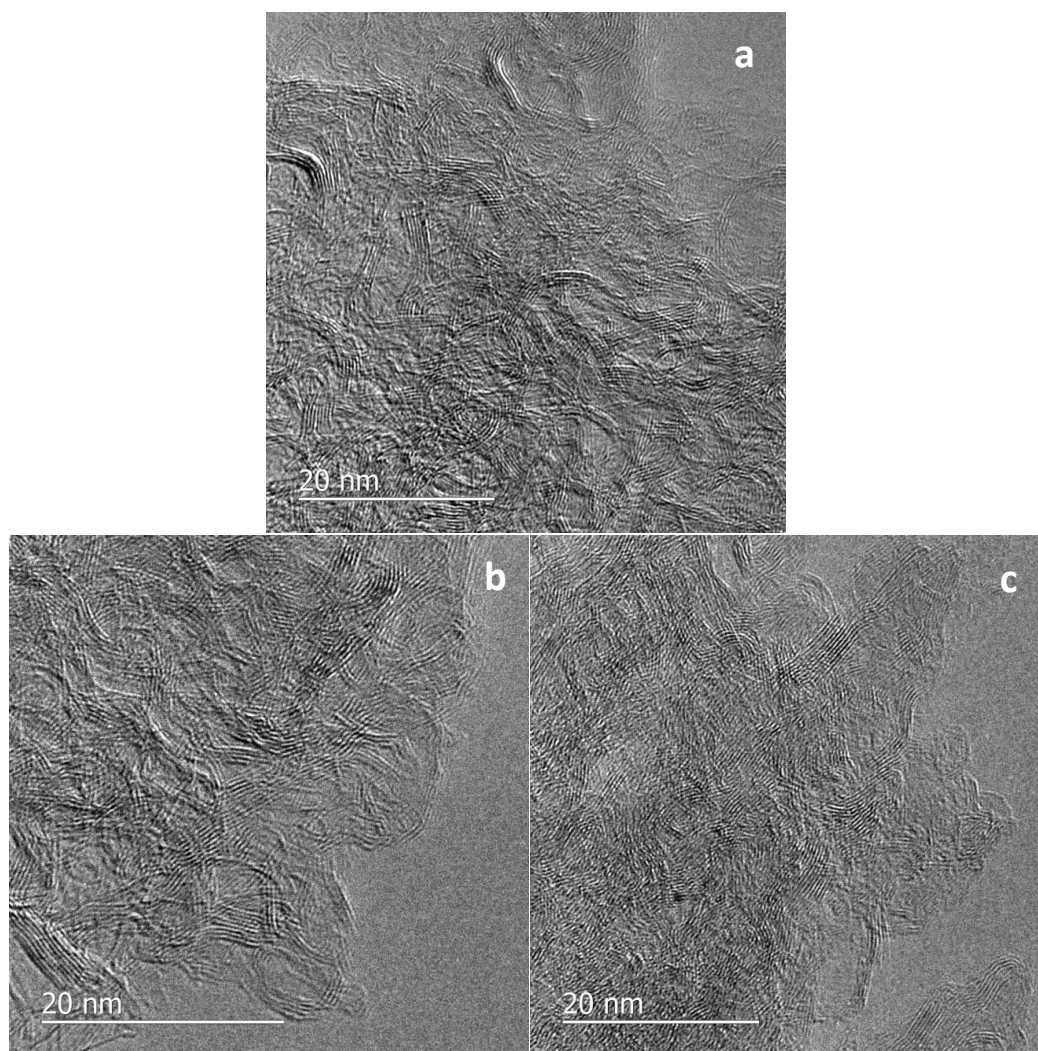
Supplementary Figure 2 | Compressional and shear wave signals (a, b, c) and corresponding X-ray radiography images of type-II glass-like carbon (GC) (d, e, f) at pressures of 0.59, 2.1, and 4.4 GPa, respectively. The compressional and shear wave signals are those from the interfaces at anvil/ Al_2O_3 buffer rod (R0), Al_2O_3 buffer rod/sample (R1), and sample/Cu (R2). The travel times between R1 and R2 are the two-way signals in the sample.



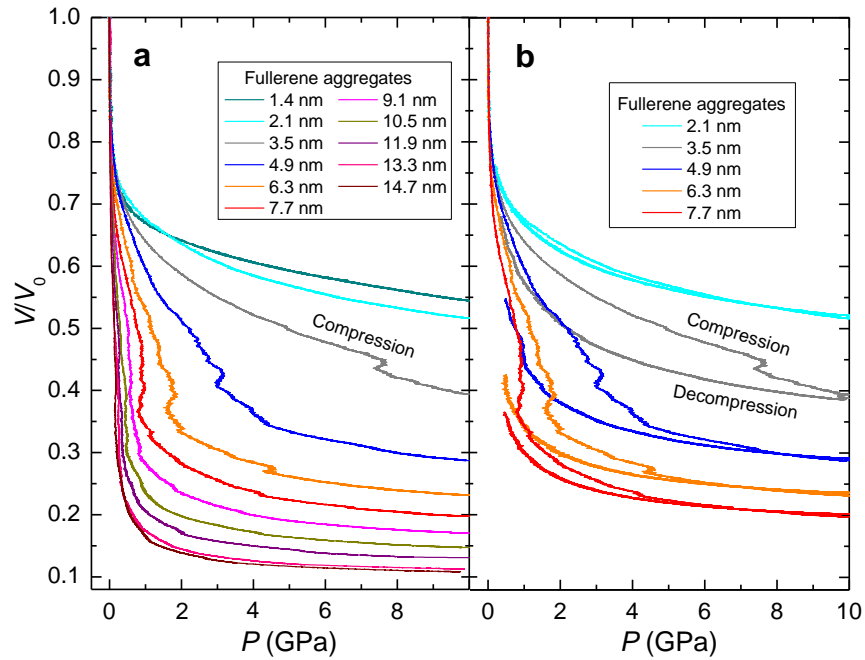
Supplementary Figure 3 | Acoustic velocities and deduced densities of type-I (solid symbols) and type-II glass-like carbons (GC) (open symbols). (a) Measured longitudinal (V_p) and shear (V_s) wave velocities at various pressures; the errors are less than 0.4%. (b) The obtained elastic moduli at various pressures; the errors are less than the size of the symbols. (c) Densities determined by integrating acoustic velocities, together with the results from optical imaging measurements. The raw materials were all in plate form.



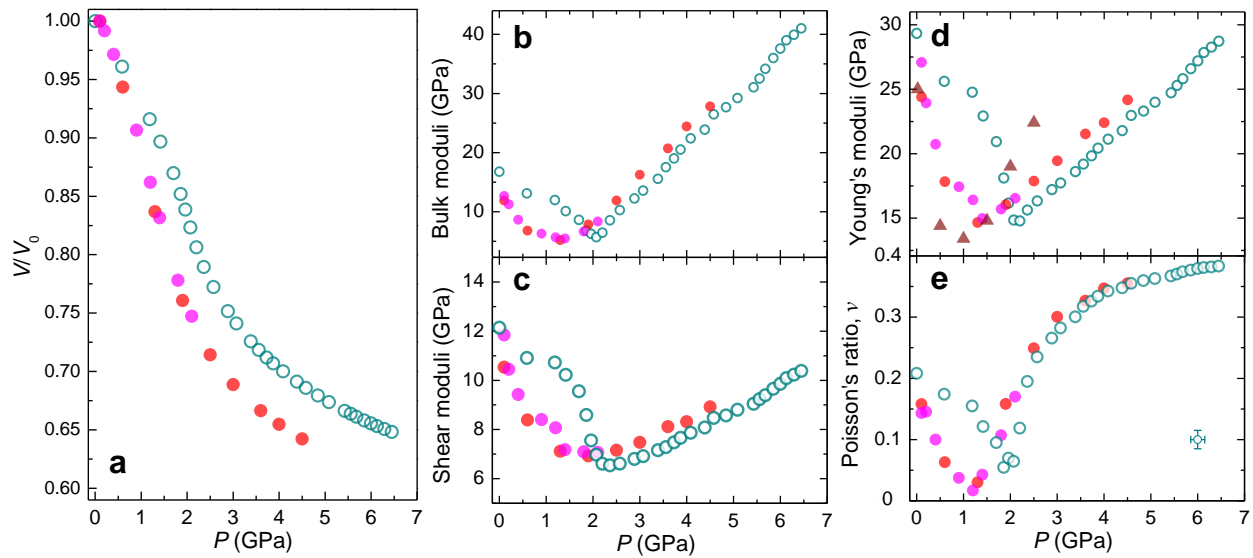
Supplementary Figure 4 | Triaxial deformation of type-II (a) and -I (b, c) glass-like carbon (GC) under high pressures. (a, b) Raw experimental data shows piston displacement versus differential stress. (c) Differential stress-axial strain curves of type-I GC at various confining pressures from 0.5 to 2.0 GPa. The linear portions (indicated by the dashed lines) are elastic, with the slopes corresponding to the Young's moduli at various pressures. Type-I GC yields at somewhat lower strains, compared to type-II GC (Fig. 3b). The raw materials were the purchased GC rods.



Supplementary Figure 5 | HRTEM images of type-II glass-like carbon (GC) samples recovered from various stages of compression. All scale bars are 20 nm. **(a)** Starting material; **(b)** recovered from 5.1 GPa; **(c)** recovered from 13.1 GPa. In both **a** and **b**, fringes of multi-graphene layers curved around fullerene-like spheroids (FLS) are seen. A comparison between **a** and **b** suggests that the sample recovered from 5.1 GPa did not experience any noticeable structural modification. In **c**, many areas lack FLS, suggesting the partial collapse of FLS after the pressure of 13.1 GPa. The closely packed and straightened fragments of multi-graphene layers indicate the sample was not recovered. These observations are consistent with the volume measurements.



Supplementary Figure 6 | Compression and decompression curves for 3D double-layer fullerene arrays with various sphere diameters according to MD simulations. The interlayer distance of double-layer fullerene is 0.34 nm for the initial modeling. For simplify, only the outer diameters are marked. For example, the 1.4 nm outer diameter fullerene has inner diameter of 0.7 nm. **(a)** Compression curves of fullerene arrays with sphere diameters from 0.7 to 14.7 nm. A cusp is observed in the compression curves when fullerene diameters are above 3.5 nm, and the cusps occur at lower pressures for fullerenes with larger diameters. **(b)** Compression and decompression curves of selected fullerene arrays. The large diameter fullerene arrays collapse and experience permanent plastic deformation at the jerk pressures, which contrasts the observed elastic recovery of GC with fullerene diameter of 5-10 nm.



Supplementary Figure 7 | Pressure-induced property changes of various type-II glass-like carbon (GC) samples. (a) Compression data based on the ultrasonic velocity measurements. (b,c,d,e) Bulk, shear, Young's moduli, and Poisson's ratio changes under pressure. In d, circles represent data obtained by ultrasonic velocity measurements; triangles are those obtained from the stress-strain relationship in triaxial deformation experiments of GC rods (Fig. 3 and Supplementary Figure S4). Solid magenta and red circles are those obtained from GC rod samples, and open circles are those from GC plate samples (see also Fig. 2). The different type-II GC samples show slightly different compressibility, pressure-tunable elastic moduli, and Poisson's ratios.